Unidirectional Ultra-Long Distributed Optical Fiber Sensor

Yaxi Yan, Hua Zheng, Alan Pak Tau Lau, Changjian Guo, and Chao Lu

***Abstract*—In this paper, we propose and experimentally demonstrate an ultra-long distributed fiber vibration sensing system using unidirectional forward transmission of a continuous-wave signal and coherent detection with digital signal processing. Two optical fibers, which are close to each other, are deployed for sensing. A loop-back configuration is formed by splicing these two optical fibers at the far end of these two fibers. The location of the vibration event is identified by analyzing the null points in the frequency spectrum of the extracted phase signal. Thanks to the nature of unidirectional forward transmission, the Rayleigh backscattering noise can be avoided. Meanwhile, forward transmission enables optical amplifiers to compensate for the signal loss and hence fundamentally overcome the sensing range limit. We successfully demonstrate the localization of single point and multi-point vibrations with measurement errors of less than $\pm$100 m and $\pm$200 m, respectively, over a 500-km sensing range. The proposed scheme opens new possibilities in ultra-long haul distributed optical sensing applications.**

***Index Terms*—Ultra-long haul, forward transmission, distributed vibration sensor.**

I. INTRODUCTION

DISTRIBUTED vibration sensing (DVS) using optical fibers has been widely applied in many engineering areas including structural health monitoring, oil or gas pipeline leakage monitoring, perimeter protection and seismic sensing applications [1]–[5]. Among them, because of the advantages of high sensitivity, fast response and simple structure, distributed interferometer sensors, including Mach-Zehnder interferometer (MZI) [6], Michelson interferometer [7], Sagnac interferometer [8] and hybrid interferometer structures [9]–[10], have attracted much research attention and have been extensively studied over the past decades. In interferometer-based DVS systems, light beams are bidirectionally transmitted in a single fiber. Because of this bidirectional transmission, traditional distributed interferometer sensor is influenced by the Rayleigh backscattering noise (RBN), which limits the sensing range [11]. In [12], wavelength division multiplexing (WDM) was utilized to reduce the influence of RBN in the Mach Zehnder interferometer, which resulted in a more complicated sensing structure. Besides, in MZI systems, the optical delay is wavelength dependent. As a result, in MZI systems with WDM techniques, the deviation of the location information obtained using the time delay estimation method increases with the increase of the sensing distance. Recently, a Michelson interferometer using polarization beam splitter and Faraday rotating mirror (FRM) was reported [7]. 2/3 of the RBN can be removed, however, the residual RBN still degrades the signal to noise ratio (SNR), especially in long range sensing systems. In traditional interferometer based DVS systems, direct detection is normally used at the receiver. The directly detected signal exhibits a nonlinear phase to amplitude conversion, which results in a serious distortion of the sensing signal. This is especially serious when the vibration amplitude is large or the interferometer sensor is not fixed at the quadrature working point [13]. To solve this problem, various phase detection techniques including phase carrier generation [14] and the use of 3$\times$3 coupler [15], are utilized in interferometer based DVS. These techniques, however, may result in a complicated signal processing infrastructure which increases the system complexity and measurement time. Besides, interferometer DVS suffers from the polarization fading effect as well. In most cases of interferometer based DVS systems, additional polarization control is necessary to solve the polarization fading problem, which increases the complexity of the system as well. However, the polarization fading problem can be easily solved by using the phase and polarization diversity coherent receiver, which has been widely used in long-haul optical communication systems [16] and OTDR based sensing systems [17] to retrieve both the amplitude and phase of the received signal.

With a more extensive application of fiber sensing technology, there is an increasing demand for the long range and ultra-long range fiber vibration sensing in many application areas. In our previous work, a unidirectional forward transmission-based distributed vibration sensor using phase and polarization diversity

Manuscript received May 3, 2021; revised July 12, 2021; accepted July 15, 2021. Date of publication July 21, 2021; date of current version August 11, 2021. The work was supported in part by the National Key R&D Program of China under Grant 2018YFB1801700, in part by the Science and Technology Program of Guangzhou under Grant 2019050001, in part by the Guangdong Natural Science Foundation under Grant 2018A0303130117, and in part by the Science and Technology Planning Project of Guangdong Province, China under Grant 2019A050510039. *(Corresponding author: Changjian Guo.)*

Yaxi Yan and Hua Zheng are with the Department of Electronic and Information Engineering, The Hong Kong Polytechnic University, Hung Hom, Hong Kong (e-mail: ya.xi.yan@connect.polyu.hk; hua.zheng@polyu.edu.hk).

Alan Pak Tau Lau is with the Department of Electrical Engineering, The Hong Kong Polytechnic University, Hung Hom, Hong Kong, and also with The Hong Kong Polytechnic University Shenzhen Research Institute, Shenzhen 518057, China (e-mail: eeaptlau@polyu.edu.hk).

Changjian Guo is with the South China Academy of Advanced Optoelectronics, South China Normal University, Guangzhou 510006, China, and also with the Department of Electrical Engineering, The Hong Kong Polytechnic University, Hung Hom, Hong Kong (e-mail: changjian.guo@coer-scnu.org).

Chao Lu is with the Department of Electronic and Information Engineering, The Hong Kong Polytechnic University, Hung Hom, Hong Kong, and also with The Hong Kong Polytechnic University Shenzhen Research Institute, Shenzhen 518057, China (e-mail: enluchao@polyu.edu.hk).

Digital Object Identifier 10.1109/JPHOT.2021.3098634

coherent detection was proposed to realize an over 600 km sensing range [18]. In the proposed scheme, a frequency-shifted optical delay line (FSODL) is used so that two differential phase signals can be constructed. Consequently, the vibration location is obtained by measuring the time delay between two differential phase signals. Multi-point detection is imperative for DVS systems. Although it is demonstrated in [18] that multi-point vibration can be realized through time delay estimation, it is only possible when following conditions: 1). vibration positions are far away; 2). vibration signals are uncorrelated and 3) the power difference between different vibration signals is not very big; are satisfied simultaneously. Besides, the sampling rate of the previous proposed sensing system must be at least twice as high as the frequency shift induced by the acousto optic modulator due to the use of FSODL, which largely increases the load of data processing. In this work, we have shown that the location information can be obtained by analyzing the null point in the frequency spectrum. This is a more powerful approach for multi-point sensing. At the same time, the sensing structure can be further simplified by removing the FSODL structure, which makes the sensing system more cost-effective. Besides, the load of data processing can be largely reduced since only processing of baseband signal is required. Here a simplified ultra-long range unidirectional forward transmission based DVS is proposed and experimentally demonstrated. A pair of multi-span optical fibers are utilized for sensing while a loop-back configuration is used by connecting the two fibers at the far end. A commercial phase- and polarization-diversity coherent receiver is used to extract the phase information from the received signal after the forward transmission. Because the pair of sensing fibers are deployed close to each other, same phase change patterns will occur in case of disturbance events. The sensing of the external vibration is realized by demodulating the phase signal of the received light while the localization of the vibration event is realized by analyzing the null points displayed in the spectrum of the phase signal after fast Fourier transform (FFT). The proposed scheme eliminates the RBN problem with a simple sensing structure. The sensing performance of a 1000 km fiber link is investigated, corresponding to a sensing range of 500 km. The location performance of both single-point vibration and multi-point vibration is analyzed in detail. Results show that the location error of single point vibrations is less than ± 100 m while the location error of multi-point vibrations is less than ± 200 m. Taking advantages of optical amplification, the sensing distance can be further extended. The proposed scheme provides a new approach for ultralong range and large amplitude DVS sensing.

II. Experiment Setup and Sensing Principle

A. Experimental Setup

The experimental setup of the proposed distributed vibration sensor is schematically shown in Fig. 1. The output of an ultra-narrow-linewidth CW tunable laser operating at 1550 nm (NKT KOHERAS ADJUSTIK X15) was split into two branches. The upper branch was launched into the fiber under test (FUT) directly for sensing. The lower branch serves as a local oscillator

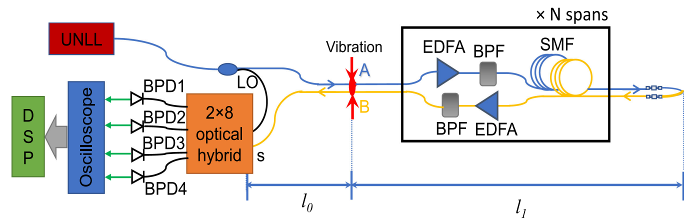

Fig. 1. Experiment setup of the proposed ultra-long distributed vibration sensing scheme. UNLL: ultra-narrow linewidth laser; EDFA: erbium doped fiber amplifier; BPF: band-pass filter; SMF: single mode fiber; LO: local oscillator; BPD: balanced photodetector; DSP: digital signal processing.

(LO). The FUT was a 1000 km fiber link, consisting of 14 spans of standard single-mode fiber (SSMF, G.652D). An EDFA (Huawei C-band OAU) and a 4-nm band pass filter (BPF) were utilized in each span to compensate the loss induced by the fiber and to remove the out-of-band ASE noise, respectively. In our sensing scheme, the FUT was composed of a pair of equal-length fibers and these two fibers were placed close to each other to ensure the same external vibration induced phase change of the propagation light. Without loss of generality, parts of two fibers, where the external vibrations were applied, were glued together to simplify the experiment procedure. The far ends of two fibers are spliced together to form a loop-back arrangement. After propagating through the 1000 km fiber link, a polarization-diversity homodyne coherent receiver consisting of an optical 90° hybrid mixer (PHOTOP C-band 2×8) and four balanced photodetectors with 500 MHz bandwidth were used to detect the beating signals between the output signal light and LO. By using a digital oscilloscope (PicoScope 6404B), the detected analog signal was digitized and then transferred to a computer for further signal processing.

B. Sensing Principle

At the output of the polarization-diversity coherent receiver, the in-phase (Ix, Iy) and quadrature (Qx, Qy) components of the beating signals in both x- and y- polarizations can be detected and expressed as

$$I_x = R\sqrt{\frac{\alpha P_S P_{LO}}{2}}\cos\left(\varphi_x(t) - \varphi_{LO}(t) + \delta\right) \quad (1)$$

$$Q_x = R\sqrt{\frac{\alpha P_S P_{LO}}{2}}\sin\left(\varphi_x(t) - \varphi_{LO}(t) + \delta\right) \quad (2)$$

$$I_y = R\sqrt{\frac{(1-\alpha) P_S P_{LO}}{2}}\cos\left(\varphi_y(t) - \varphi_{LO}(t)\right) \quad (3)$$

$$Q_y = R\sqrt{\frac{(1-\alpha) P_S P_{LO}}{2}}\sin\left(\varphi_y(t) - \varphi_{LO}(t)\right) \quad (4)$$

where P_S and P_{LO} are the powers of the signal light and LO, respectively; R is the responsivity of the photodetectors in the coherent receiver; α is the power ratio of the two polarization components while δ is the phase difference between them; $\varphi_x(t)$, $\varphi_y(t)$ and $\varphi_{LO}(t)$ are the phases of signal along x-polarization, signal along y-polarization and LO, respectively. Through applying the IQ demodulation algorithm to (1) to (4), the phase of the signal light can be obtained [19].

If a vibration occurs at a certain position of the fiber link, the refractive index of the fiber core and the fiber birefringence will be changed accordingly. As a result, the phase of the light will be modulated when passing through the vibration position. Due to the loop-back configuration, a single external vibration will affect the propagation light twice, marked as points A and B in Fig. 1. Therefore, the demodulated phase signal in this experiment can be written as

$$\varphi(t) = \varphi_c(t) + \varphi_n(t) + \varphi_v(t) + \varphi_v(t-\tau) \tag{5}$$

where $\varphi_c(t)$ is the carrier phase noise related to the linewidth of the laser source; $\varphi_n(t)$ is the phase noise accumulated along the propagation path, which includes the phase change caused by thermal variations, acoustic waves, background mechanical disturbance, etc.; $\varphi_v(t)$ is the phase term modulated by the external vibration; τ is the time for light to transmit from disturbance point A to disturbance point B, which can be written as

$$\tau = 2nl_1/c \tag{6}$$

where *n* is the refractive index of the fiber core.

The spectral component of the demodulated phase signal can be analyzed in the frequency domain. We denote the FFT of $\varphi(t)$ as $\hat{\varphi}(f)$, which can be derived as

$$\hat{\varphi}(f) = \underset{c}{\hat{\varphi}}(f) + \underset{n}{\hat{\varphi}}(f) + \underset{v}{\hat{\varphi}}(f)(1 + e^{-j2\pi f\tau}) \tag{7}$$

When the following condition is satisfied:

$$2\pi f\tau = (2k+1)\pi, k\text{is an integer} \tag{8}$$

we have

$$\hat{\varphi}(f) = \underset{c}{\hat{\varphi}}(f) + \underset{n}{\hat{\varphi}}(f) \tag{9}$$

That means the phase change caused by external vibrations is zero for certain vibration frequencies. In other words, there will be a series of null points in the frequency spectrum of $\varphi(t)$ and the frequency of the null point is related to the location of the external vibration, which can be derived from (6) and (8) as

$$f_{k^{th}null} = \left(\frac{k}{2} + \frac{1}{4}\right)\frac{c}{nl_1} \tag{10}$$

The frequency interval between two consecutive null points can be derived as

$$\Delta f_{null} = c/2nl_1 \tag{11}$$

Therefore, the length of l_1 can be obtained by determining the frequency interval between two consecutive null points. As the total length of the sensing fiber is already known, the location of the vibration can be finally determined.

There are two ways to determine the frequency interval Δf_{null}. Referring to (10) and (11), the frequency interval can be determined by

$$\Delta f_{null} = f_{k^{th}null}/(k+0.5) \tag{12}$$

Therefore, one method is to determine the frequency of the k^{th} null point first. Then the frequency interval Δf_{null} can be calculated using (12). The detailed processing procedures are:

1) Apply an adaptive digital low pass filter to remove the high frequency noise of the frequency signal $\hat{\varphi}(f)$ and then obtain a smooth frequency curve where null points are clearly displayed;
2) Roughly determine the frequency interval Δf_{rough} by subtracting the frequency values of two consecutive null points;
3) Choose a null point with sharp dip and find out the corresponding frequency value $f_{k^{th}null}$;
4) Determine the integer *k* by rounding the value calculated by $(f_{k^{th}null}/\Delta f_{rough} - 0.5)$;
5) Finally determine the frequency interval using (12).

According to (10), the measured location can be expressed as

$$l_1 = c(k+0.5)/2nf_{k^{th}null} \tag{13}$$

The measurement variance of the location can then be written as

$$\begin{aligned}\Delta l_1 &= c\Delta f_{k^{th}null}(k+0.5)/2nf^2_{k^{th}null} \\ &= c\Delta f_{k^{th}null}/2n\Delta f_{null} f_{k^{th}null}\end{aligned} \tag{14}$$

where $\Delta f_{k^{th}null}$ is the measurement variance of the k^{th} null frequency. It is obvious that the location accuracy is linearly related to the measurement variance $\Delta f_{k^{th}null}$, however, inversely proportional to Δf_{null} and the frequency of k^{th} null point.

The other method is using the double FFT algorithm [20], in which a second time FFT is applied to the frequency spectrum of the phase signal. The frequency interval between two consecutive null points is determined by figuring out the peak in the second time FFT spectrum. In our case, the detailed processing procedures are

1) A section of the sensing signal is obtained from the scope; the spectral component, $\hat{\varphi}(f)$, of the demodulated phase signal is calculated.
2) Because the power of the phase noise is inversely proportional to the noise frequency, there is a downtrend on the calculated frequency signal $\hat{\varphi}(f)$. Therefore, the downtrend *D*(*f*) is first obtained by fitting the curve $\hat{\varphi}(f)$.
3) Remove the downtrend of by subtracting *D*(*f*) from $\hat{\varphi}(f)$.
4) A section of $\hat{\varphi}(f)$ after removing the downtrend that contains the effective information is obtained.
5) To enhance the resolution of the second time FFT spectrum, zeros are padded to the end of the first time FFT signal.
6) Apply second time FFT to the processed first time FFT signal.
7) Estimate the value of the spectral peak shown in the second time FFT spectra.

In the double FFT method, assuming that the frequency range and the data length of the first time FFT signal after zero padding are *F* and *L* respectively, the x coordinate of the second time FFT spectrum will value from -*L*/2 to *L*/2-1. In that case, when the

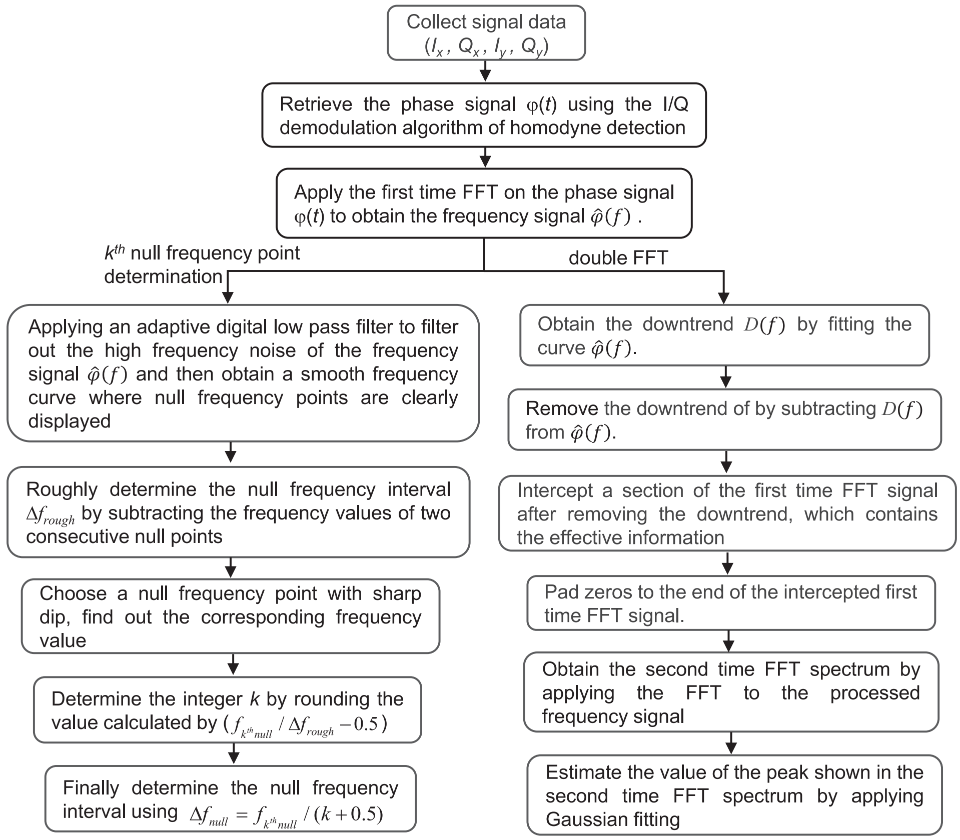

Fig. 2. The flow chart of the data processing procedures of two location methods.

x value of the peak in the second time FFT spectra is P, the corresponding frequency interval between two consecutive null points should be

$$\Delta f_{null} = F/P \tag{15}$$

According to (11) and (15), the vibration location should be

$$l_1 = cP/2nF \tag{16}$$

That means the measurement variance of the location is

$$\Delta l_1 = c\Delta P/2nF \tag{17}$$

where ΔP is the measurement variance of P. To estimate the peak value more precisely, Gaussian fitting can be applied on the second time FFT curve. In this work, both of these two location methods were used to investigate the sensing performance and comparisons between these two methods were conducted as well. Fig. 2 shows the data processing procedures of these two methods.

III. Results and Discussions

A. Location Result of Single-Point Vibration

A proof-of-concept experiment is conducted to investigate the sensing performance of the proposed DVS. Firstly, single point vibration was investigated. In order to emulate the practical circumstance, vibrations were separately applied at three different positions, i.e., 500km, 200 km and 12.5 km from the loop center of the fiber link. The vibration signal was introduced by continuously hammering a fiber spool, which is wrapped by two 10 m single mode fibers that are glued together. The collection time was 10 s for a single shot sampling and the sampling rate was set as 4.8 MSa/s. The phase signal retrieved from the collected data is shown in Fig. 3, where obvious phase changes can be found when external vibrations occur. As the hammering continues, a series of peaks can be observed on the phase curve, whose intervals are corresponding to the hammering period. One may also find from Fig. 3 that the phase of the received signal slowly fluctuates even before vibration was applied. This may be attributed to the following causes: 1) environment temperature fluctuation, which may induce length variations of the optical path; 2) acoustic noise along the propagation path and, 3) the

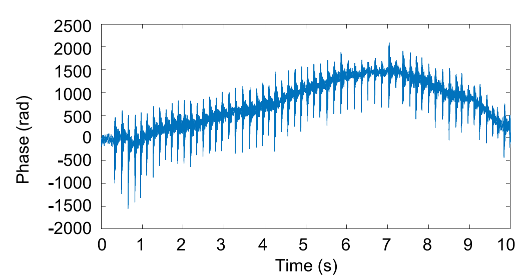

Fig. 3. The demodulated phase signal when hammering disturbance is applied at the position of 200 km.

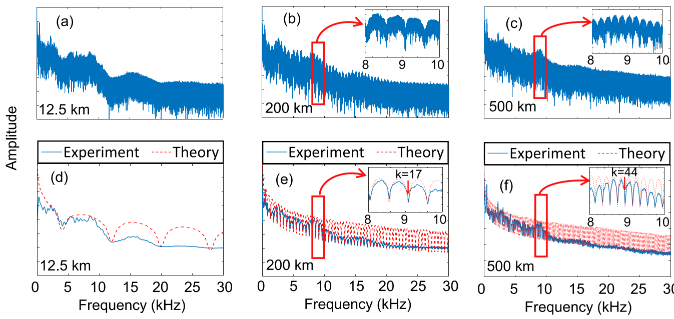

Fig. 4 (a), (b) and (c) are original frequency spectra of the demodulated phase signals when disturbance is applied at positions of 12.5 km, 200 km and 500km, respectively. (d), (e) and (f) are frequency spectra obtained by applying a low pass filter on (a), (b) and (c), respectively, where the theoretical response (red dotted lines) and experimental results (blue solid lines) are not consistent in amplitude.

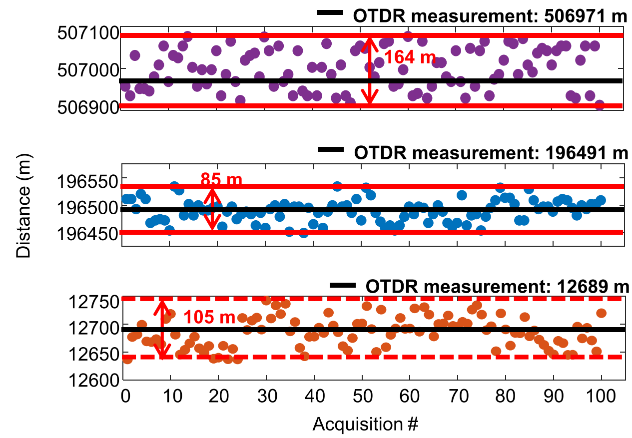

Fig. 5. The location results obtained by using the kth null frequency determination method when vibrations occur at three different vibration positions.

carrier phase noise. By applying FFT to the demodulated phase signal, the frequency spectrum can be obtained. Fig. 4 shows the frequency spectra of the demodulated phase signals after FFT when vibrations were applied at three different positions. A series of dips (null points) appear in the spectra. The key point of locating the external vibration is to determine the frequency interval between two consecutive null points precisely.

For the k^{th} null point determination method [referring to (14)], the measurement error of the k^{th} null frequency will have a dramatic impact on the accuracy of location. Therefore, an adaptive low pass filter was used to remove the high frequency noise to reduce the measurement error. Figs. 4(d-f) show the finally obtained null-frequency curves after removing the high-frequency noise. Since the measurement accuracy is inversely proportional to the value of k^{th} null frequency, a large value of k^{th} null frequency helps to reduce the measurement error. Besides, from Fig. 4(e) and (f), the first time FFT signals have high SNRs near the frequency of 9 kHz. Therefore, the value of k^{th} null frequency in this experiment is chosen around 9 kHz.

As shown in Fig 4(f), for the position of 500 km, the 45th null point ($k = 44$) was chosen to determine the frequency interval. As shown in Fig. 4(e), for the position of 200 km, the 18th null point ($k = 17$) was chosen. When the vibration occurs at the position of 12.5 km, as shown in fig. 4(d), there is just two null points in the spectrum and only the first null point is sharp and clear, so the first null point was chosen for the localization. To investigate the location error of this sensing scheme, the knocking test on the above mentioned three different positions of the fiber link were all repeated 100 times. Fig. 5 shows the location results. Each vibration position was measured by a commercially available OTDR with a resolution of 5 m as a reference. Compared with the results obtained by using OTDR, one can see that the location error is less than $\pm$ 100 m. As for the location results of vibrations occurring at the 12.5 km position, even though the null frequency dip is not sharp, because the null frequency interval is very large, the measurement error is not very big, even smaller than that of vibrations occurring at the 500 km position.

Next, the double FFT algorithm was used to process the data as well. In this work, the effective frequency range of the first time FFT signal was from 0 Hz to 30 kHz. Since the effective

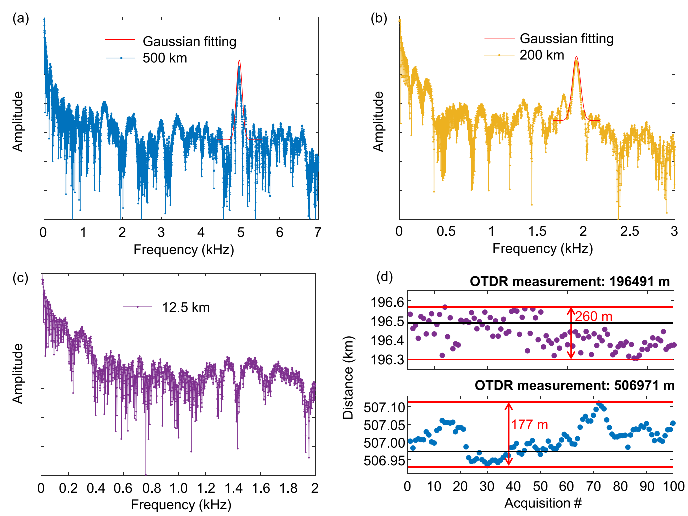

Fig. 6. The second time FFT spectra obtained by applying the FFT on the first time FFT signals $\hat{\varphi}(f)$ when single-point vibrations occur at three different positions (a) 500 km, (b) 200 km and (c) 12.5 km, respectively. (d) Location results obtained by using the double FFT algorithm when vibrations occur at positions of 200 km and 500 km.

frequency range of the first time FFT signal is not wide enough, zero padding is used to increase the resolution of the second time FFT spectrum. It should be noted that when the resolution of the second time FFT spectrum is high enough, the location accuracy is only determined by the system's noise and the effective length of the original data. Moreover, longer padding zeros means the increase of the computational complexity. Therefore, there is an optimal length of padding zeros. In this work, the frequency range of the signal used for the second time FFT is extended to 0 Hz -1 MHz. Figs. 6(a) (b) and (c) show the obtained spectra after the second time FFT when vibrations occur at three different positions. From Fig. 6(c), one can see that the peak in the second time FFT spectrum for vibrations occur at the position of 12.5 km is not obvious. That is because there are only 3 null points in the frequency range of 30 kHz, which is not enough for the second time FFT. One can therefore deduce that the double

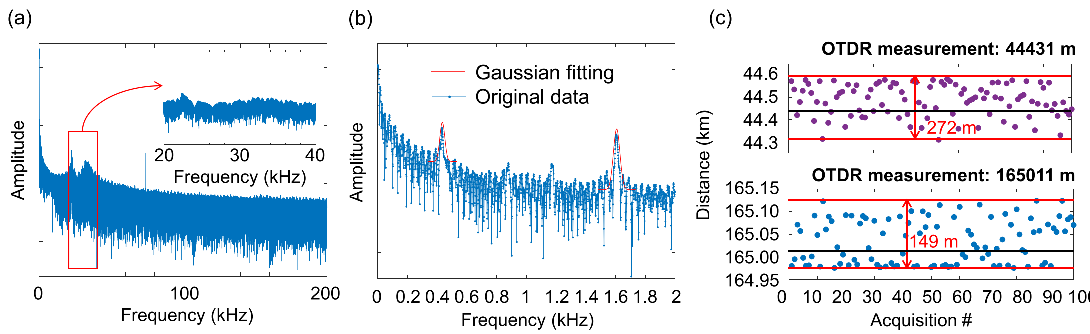

Fig. 7. (a) A zoomed region of the frequency spectra of the demodulated phase signals when vibrations occur at two different points simultaneously. (Inset) the whole spectra. (b) The second time FFT spectra. (c) The location results obtained by using the double FFT algorithm when vibrations occur simultaneously at positions of 45 km and 165 km.

FFT algorithm is valid when 1) a vibration signal with a wider frequency range is applied; and/or 2) vibrations are occurring farther away from the loop center. As shown in Figs. 6 (a) and (b), by applying Gaussian fitting, the value of the peak in the second time FFT spectrum can be determined. The location can thus be calculated using (16). Fig. 6(d) shows the location results obtained by using the double FFT algorithm. The location error of the double FFT algorithm is less than ± 200 m, which is larger than that of the k^{th} null frequency point determination method. The reason is that the location accuracy obtained using the double FFT algorithm is related to the frequency span of the vibration signal. A small frequency span of the hammering events, which is 30 kHz in our case, leads to a large location error. Besides, the double FFT algorithm is not effective for vibration events occurring close to the loop center of the fiber link. Comparing the k^{th} null frequency determination method and the double FFT algorithm, it is obvious that the k^{th} null frequency determination method is more appropriate for single point vibration detection.

B. Location Result of Multi-Point Vibrations

For single-point vibration cases, the location can be easily obtained by finding out the frequency interval between two consecutive null points as mentioned above. However, in practical ultra-long distance sensing systems, multiple vibrations may occur simultaneously at different positions along the sensing fiber. For multi-point vibration cases, the demodulated phase is the superimposing of multiple vibration signals. In that case, the frequency spectrum of the demodulated phase after FFT should be written as

$$\hat{\varphi}(f) = \hat{\varphi}_c(f) + \hat{\varphi}_n(f) + \sum_{m=1}^{N} \hat{\varphi}_{\phi_m}(f)(1 + e^{-j2\pi f\tau_m}) \quad (18)$$

where m represents the m^{th} vibration position and N is the total number of vibration positions. To investigate the multi-point vibration sensing performance, two PZTs are placed at positions of 45 km and 165 km from the loop center of the fiber link. Two 10 m fibers are wrapped around these two PZTs, separately. Vibrations are introduced by driving the PZTs using two random Gaussian-noise-like electrical signals both with a peak to peak voltage of 10 V. Fig. 7(a) shows the frequency spectrum when two vibrations occur simultaneously. Because the retrieved phase signal is a superposition of two vibration signals, the null points in the spectrum are indistinctive. In such cases, only the double FFT algorithm can be used to determine the frequency interval effectively.

Here, the frequency range of the zero padded first time FFT signal used for second time FFT was from 0 Hz to 1 MHz as well. Fig. 7(b) shows the result after the second time FFT. There are two peaks shown in the spectra, representing two vibration positions. The exact value of each peak is determined by using Gaussian fitting. Fig. 7(c) shows the location results of 100 times repetitive tests. The location error is less than ± 200 m. Location of two-point vibrations has been verified in this work and it is obvious that the double FFT method can be used for multi-point (larger than two) vibrations as well.

From location results of both the single-point vibrations and multi-point vibrations using the double FFT algorithm, it is obvious that the location accuracy deteriorates when the vibration position moves towards the loop center of the fiber link. That is because the vibration occurring farther away from the loop center has a higher SNR of the spectral peak shown in the second time FFT spectra. Besides, in this experiment, the location accuracies of multi-point vibrations were overall higher than those of single-point vibrations obtained based on the double FFT algorithm. That is because a larger effective frequency ranging from 0 Hz to 200 kHz as shown in Fig. 7(a) is obtained in multi-point vibration localization. It should be noted that the location accuracy can be further enhanced by improving the SNR of the first time FFT signals through averaging.

IV. Conclusion

In this work, we have proposed and experimentally demonstrated a unidirectional ultra-long range distributed optical vibration sensing technique using coherent detection, where a pair of optical fibers are deployed at the same location with a loop-back configuration. Both the k^{th} null frequency determination method and double FFT algorithm have been used to investigate the sensing performance. Less than ± 100 m location error of single point vibrations and less than ± 200 m location error of multi point vibrations have been realized over a 500 km sensing range. Compared with previously reported distributed vibration sensors, the proposed scheme has a much simpler structure. Meanwhile, with the help of EDFAs and the elimination of the Rayleigh backscattering noise, the sensing distance can be further extended, which enables ultra-long distributed vibration sensing. In practical applications, like perimeter security systems and railway tunnel monitoring systems, actions like knocking, hammering, digging and climbing will generate vibrations with wide frequency span. With the development of the infrastructure and the need for long distance transportation, the proposed scheme has a great potential in ultra-long range DVS applications.

References

[1] M. Lopez-Higuera, L. R. Cobo, A. Q. Incera, and A. Cobo, "Fiber optic sensors in structural health monitoring," *J. Lightw. Technol.*, vol. 29, no. 4, pp. 587–608, Feb. 2011.

[2] S. Liang *et al.*, "Fiber-optic intrinsic distributed acoustic emission sensor for large structure health monitoring," *Opt. Lett.*, vol. 34, no. 12, pp. 1858–1860, Jun. 2009.

[3] X. Li, Q. Sun, J. Wo, M. Zhang, and D. Liu, "Hybrid TDM/WDM-based fiber-optic sensor network for perimeter intrusion detection," *J. Lightw. Technol.*, vol. 30, no. 8, pp. 1113–1119, Apr. 2012.

[4] A. Sladen *et al.*, "Distributed sensing of earthquakes and ocean-solid earth interactions on seafloor telecom cables," *Nat. Commun.*, vol. 10, no. 1 pp. 1–8, Dec. 2019.

[5] G. Marra *et al.*, "Ultrastable laser interferometry for earthquake detection with terrestrial and submarine cables," *Science*, vol. 361, no. 6401, pp. 486–490, Aug. 2018.

[6] Q. Sun, D. Liu, J. Wang, and H. Liu, "Distributed fiber-optic vibration sensor using a ring Mach-Zehnder interferometer," *Opt. Commun.*, vol. 281, no. 6, pp. 1538–1544, Mar. 2008.

[7] Q. Song, H. Peng, S. Zhou, P. Zhou, Q. Xiao, and B. Jia, "A novel weak-scattering michelson interferometer based on PBS for long-distance disturbance localization," *J. Lightw. Technol.*, vol. 38, no. 8, pp. 1543–1549, Nov. 2019.

[8] F. Teng, D. Yi, X. M. Hong, and X. J. Li, "Distributed fiber optics disturbance sensor using a dual-Sagnac interferometer," *Opt. Lett.*, vol. 44, no. 20, pp. 5101–5103, Oct. 2019.

[9] Q. Song *et al.*, "Improved localization algorithm for distributed fiber-optic sensor based on merged Michelson-Sagnac interferometer," *Opt. Exp.*, vol. 28, no. 5, pp. 7207–7220, Mar. 2020.

[10] S. Wang, P. Lu, L. Mao, D. Liu, and S. Jiang, "Cascaded interferometers structure based on dual-pass Mach–Zehnder interferometer and sagnac interferometer for dual-parameter sensing," *Opt. Exp.*, vol. 23, no. 2, pp. 674–680, Jan. 2015.

[11] G. A. Cranch, A. Dandridge, and C. K. Kirkendall, "Suppression of double Rayleigh scattering-induced excess noise in remotely interrogated fiber-optic interferometric sensors," *IEEE Photon. Technol. Lett.*, vol. 15, no. 11, pp. 1582–1584, Oct. 2003.

[12] C. Ma *et al.*, "Long range distributed fiber vibration sensor using an asymmetric dual Mach–Zehnder interferometers," *J. Lightw. Technol.*, vol. 34, no. 9, pp. 2235–2239, May 2016.

[13] Z. Zhao, M. Tang, L. Wang, N. Guo, H.-Y. Tam, and C. Lu, "Distributed vibration sensor based on space-division multiplexed reflectometer and interferometer in multicore fiber," *J. Lightw. Technol.*, vol. 36, no. 24, pp. 5764–5772, Dec. 2018.

[14] Y. Li *et al.*, "Interferometric vibration sensor using phase-generated carrier method," *Appl. Opt.*, vol. 52, no. 25, pp. 6359–6363, Sep. 2013.

[15] K. P. Koo, A. B. Tveten, and A. Dandridge, "Passive stabilization scheme for fiber interferometers using (3×3) fiber directional couplers," *Appl. Phys. Lett.*, vol. 41, no. 7, pp. 616–618, Oct. 1982.

[16] D. S. Ly-Gagnon, K. Katoh, and K. Kikuchi, "Unrepeatered optical transmission of 20 Gb/s quadrature phase-shift keying signals over 210 km using homodyne phase-diversity receiver and digital signal processing," *Electron. Lett.*, vol. 41, no. 4, pp. 206–207, Feb. 2005.

[17] Z. Wang *et al.*, "Coherent Φ-OTDR based on I/Q demodulation and homodyne detection," *Opt. Exp.*, vol. 24, no. 2, pp. 853–858, Jan. 2016.

[18] Y. Yan, F. Nadeem Khan, B. Zhou, A. P. T. Lau, C. Lu, and C. Guo, "Forward transmission based ultra-long distributed vibration sensing with wide frequency response," *J. Lightw. Technol.*, vol. 39, no. 7, pp. 2241–2249, Apr. 2021.

[19] K. Kikuchi, "Coherent optical communication systems," in *Optical Fiber Telecommunications VB*, The Netherlands: Elsevier, 2008, pp. 95–129.

[20] H. Wang *et al.*, "Improved location algorithm for multiple intrusions in distributed Sagnac fiber sensing system," *Opt. Exp.*, vol. 22, no. 7, pp. 7587–7597, Apr. 2014.